

Long-range Static Directional Stress Transfer in a Nonlinear Elastic Crust

G. Ouillon¹ and D. Sornette^{1,2}

¹ Laboratoire de Physique de la Matière Condensée
CNRS UMR 6622 and Université de Nice-Sophia Antipolis
Parc Valrose, 06108 Nice, France
² Department of Earth and Space Sciences
and Institute of Geophysics and Planetary Physics
University of California, Los Angeles, California, USA
e-mails: Ouillon@aol.com and sornette@naxos.unice.fr

May 22, 2019

Abstract

Seeing the Earth crust as crisscrossed by faults filled with fluid at close to lithostatic pressures, we develop a model in which its elastic modulii are different in incremental tension versus compression. For a given earthquake source, such nonlinear elasticity is shown to (i) rotate, widen or narrow the different lobes of stress transfer, (ii) to modify the $1/r^2$ 2D-decay of elastic Green functions into the generalized power law $1/r^\gamma$ where $0 < \gamma \leq 2$ decreases with increasing tension-compression asymmetry and depends on the azimuth, (iii) to rotate the geometric fault plane away from the nodal moment tensor planes. Using reasonable estimates, this implies an enhancement of the range of interaction between earthquakes by a factor up to 5 – 10 and a mismatch of up to 10° – 25° between the static (geological) fault plane and the rupture plane deduced from moment tensor inversion. This may explain certain long-range earthquake triggering and hydrological anomalies in wells and suggest to revisit the standard stress transfer calculations which use linear elasticity.

There are many evidences that faults and earthquakes interact, as suggested by calculations of stress redistribution [1], elastodynamic propagation of ruptures using laboratory-based friction law [2, 3], simplified models of multiple faults [4, 5], as well as general constraints of kinematic and geometric compatibility of the deformations [6]. Maybe the simplest mechanism for earthquake interaction involves stress re-distribution, both static [7, 1] and dynamical [8] associated with a given earthquake modeled as a set of dislocations or cracks. In this simple mechanical view, earthquakes cast stress shadows in lobes of stress unloading [9, 7] and increase the probability of rupture in zones of stress increase [10], according to the laws of linear elasticity. These elastic stress transfer models are useful for their conceptual simplicity and are increasingly used [11].

However, such elastic stress transfer models seem unable to account for a growing phenomenology of long-range earthquake interactions. For instance, many large earthquakes have been preceded by an increase in the number of intermediate sized events over very broad areas [12]. The relation between these intermediate sized events and the subsequent main event has only recently been recognized on a large scale because the precursory events occur over such a large area that

they do not fit prior definitions of foreshocks [13]. In particular, the 11 earthquakes in California with magnitudes greater than 6.8 in the last century are associated with an increase of precursory intermediate magnitude earthquakes measured in a running time window of five years [14]. What is strange about the result is that the precursory pattern occurred with distances of the order of 300 to 500 km from the future epicenter, *i.e.* at distances up to ten times larger than the size of the future earthquake rupture. Furthermore, the increased intermediate magnitude activity switched off rapidly after a big earthquake in about half of the cases. This implies that stress changes due to an earthquake of rupture dimension as small as 35 km can influence the stress distribution to distances more than ten times its size. These observations of earthquake-earthquake interactions over long times and large spatial separations have been strengthened by several other works on different catalogs using a variety of techniques [15]. These results defy usual mechanical models of linear elasticity and one proposed explanation is that seismic cycles represent the approach to and retreat from a critical state of a fault network [16, 15]. Another explanation involves dynamical stress triggering [18] (see however [19]). Additional seismic, geophysical, and hydrogeological observations [20] cannot be accounted for by using models derived from the elastic stress transfer mechanism. In particular, standard poro-elastic models underestimate grossly the observed amplitudes of hydrogeological anomalous rises and drops in wells at large distances from earthquakes.

We investigate the hypothesis, and its implications for the above observations, that the crust is a nonlinear elastic medium characterized by an asymmetric response to compressive versus extensive perturbations around the lithostatic stress. This hypothesis is made on the basis of the following observations. We visualize the crust at seismogenic depth as crisscrossed by joints, cracks or faults at many different scales filled with drained fluid in contact with delocalized reservoirs at pressures close to the lithostatic pressure [21]. Indeed, a lot of data [25] collectively support the existence of significant fluid circulation to crustal depths of at least 10 – 15 km . Cracks and faults are considered to be closed rough surfaces with anfractuositites filled with fluid separated by contacts or asperities. A compressive perturbation acts on the closed cracks by stressing their asperities and the medium responds almost as an uncracked solid. Under an extensive perturbation, due to the fact that fluid pressure is almost always at rock pressure [21, 36], cracks open. As a consequence, the effective large scale elastic strength reveals the damage state of the crust and is weaker than in compression. By this mechanism, the nonlinearity is revealed for almost arbitrary small perturbations by the difference between compressive versus extensive perturbations around a mean lithostatic stress field. This is different from the ubiquitous nonlinearity of rocks, which becomes important only under large deformation [41].

To keep the analysis straightforward, we calculate the stress transfer due to a strike-slip earthquake, modeled as a standard double-couple [42], with a rupture length larger than the thickness of the seismogenic crust and we neglect the coupling between the crust and mantle. This allows to use a two-dimensional plate model, which under a standard suitable adjustment of the rigidity coefficients can also be interpreted as either in-plane strain or in-plane stress. We do not consider dynamical processes such as fluid migration or viscous flow. The mechanical plate is discretized into a square lattice with springs along the bonds of length a linking nearest neighbors and along the diagonals linking second-nearest neighbors. The diagonal springs ensure a non-vanishing shear strength [45]. The simplest and most general nonlinear property that we take into account is a weaker stiffness of the crust under tensional compared with compressional stress. This is modeled by spring stiffnesses smaller in tension than in compression by the same asymmetry ratio $0 \leq \alpha = K_t/K_c \leq 1$ for all springs [46]. It is straightforward to show that isotropic elasticity is recovered in the continuous limit in a pure compression mode (or in absence of nonlinearity for

$\alpha = 1$) when diagonal spring stiffnesses are equal to half the horizontal and vertical bond spring stiffnesses K [48], giving $\lambda = \mu = K/2$ for the two Lamé coefficients, $E = (4/3)K = (8/3)\mu$ for the Young modulus and $\nu = 1/3$ for the Poisson coefficient. We choosed $K_c = 5 \cdot 10^{14} \text{ Nm}^{-1}$ for horizontal and vertical springs so that, as we consider a plate of thickness $h = 10\text{km}$, the 3D elastic modulii used for our simulations are $E = 6.25 \cdot 10^{10} \text{ Pa}$, $\mu = 2.5 \cdot 10^{10} \text{ Pa}$, and $\nu = 0.25$, which are close to usual modulii measured in experiments. Our calculations are performed on a lattice of 200×200 times the mesh, where one mesh size corresponds to 10 km. Quantitative measurements are confined in a range between 3 and 40 mesh sizes (30 – 400 km) to minimize discrete and finite size effects.

The assumed double-couple [42] is discretized as a set of four forces of the same modulus F applied on the four nodes of a unit cell as shown in Figure 1. Taking the cell size $a = 10 \text{ km}$ comparable to the seismogenic thickness and to the rupture length, and $F = 7.1 \cdot 10^{14} \text{ N}$ corresponds to an event of scalar moment $M_0 = 7.1 \cdot 10^{18} \text{ Nm}$, i.e., of magnitude ≈ 6.5 . We impose zero displacements at the boundary of the plate of size $L \times L$ and the force field created by the double-couple is solved iteratively [49]. The stress tensor field $\sigma_{ij}(x, y)$ is then calculated as in [48].

Figure 1 (upper-left panel) shows the geometry of the double-couple defining the earthquake and the corresponding directions of the displacement calculated in a medium with asymmetric ratio $\alpha = 0.1$. The first striking result is that the square symmetry of the principal axes of the applied double-couple is broken by the displacement field, which exhibits an acute angle with the nodal planes. The amplitude of the symmetry breaking is quantified by the angle θ defined in Figure 1, which varies as a function of α as shown in Figure 2 (right panel). The reason for this symmetry breaking is that the double-couple defines two tensile and two compressive sectors. In the compressive sectors, the elastic modulii are larger, leading to an amplification of stress. This effect may have been observed in the Manyi ($Mw = 7.6$) earthquake [50]. Using SAR interferometry data, Peltzer et al. [50] interpreted the mismatch between the displacement across each side of the left-lateral strike-slip fault as due to a mechanical asymmetry between dilational and compressional quadrants. Using a first-order perturbative calculation, they estimated a coefficient $1/4 \leq \alpha \leq 1/2$ to explain the observed displacement asymmetry. The prediction of the angular mismatch θ obtained using our full non-perturbative solution in Figures 1 and 2 offers a new method for the detection and the calibration of a possible nonlinear elasticity by comparing the fault orientation with the principal axes of the seismic tensor provided by the inversion of seismic waves [51].

Figure 1 also compares the spatial field σ_{xy} for two values $\alpha = 0.5$ and $\alpha = 0.1$ with the linear case $\alpha = 1$. The lobes A, B, C and D (respectively E, F, G and H) have positive (respectively negative) σ_{xy} . Lobes E and G (respectively F and H) are oriented along the compressive (respectively extensive) sectors of the double-couple and are as a consequence amplified (respectively attenuated) by the nonlinear elasticity considered here [52]. Notice that, as α decreases, lobes E and G along the principal compressive direction have a stronger and stronger directivity, which is reminiscent of the chain force effect in granular media [53]. This defines three classes of lobes: 1) A, B, C and D characterized by a positive shear stress; 2) E and G characterized by a negative shear stress oriented along the compressive sectors of the double-couple; 3) F and H characterized by a negative shear stress oriented along the tensile sectors of the double-couple.

Figure 3 quantifies the decay of σ_{xy} with distance from the origin of the double-couple in different lobes along their crests. For $\alpha = 1$, we recover the standard power law decay $\propto 1/r^2$ with distance r . For $\alpha < 1$, we find also power law decays $\propto 1/r^\gamma$ which are different in the three different lobe classes with exponents $\gamma(\alpha)$ which decrease with α for lobes $A - D$ and E, G , and

increases with α lobes F, H [54]. The dependence of $\gamma(\alpha)$ is shown in Figure 2 (left panel). Notice that the maximum stress is approximately the same for all lobes and for all α 's very close to the source with an amplitude of the order of $0.3 - 0.6$ Mpa. At larger distances, the impact of α is striking. For $\alpha = 0.1$, the shear stress is 100 times larger at 100 rupture lengths than in the linear elastic case in the lobe class A, B, C, D , for instance. If we assume that a stress increase of the order of 0.1 bar (10^4 Pa) is sufficient to trigger an event, then an earthquake could remotely trigger another shock at a distance of about 8 times its rupture length in the linear case and at up to 40 times its rupture length for $\alpha = 0.01$. In the lobe class A, B, C, D , the exponent γ decreases sharply for $\alpha \leq 0.3$ with $\gamma(\alpha = 0.1) = 1.33$ and $\gamma(\alpha = 0.01) \approx 0.8$. In the lobe class E, G , γ decreases similarly from a value close to 2 for $\alpha = 1$ to $\gamma(\alpha = 0.01) = 1.22$. The exponent γ for lobe class E, G is not the same as in the case of lobe A , showing that both lobes are not exactly antithetic. The behaviour of lobes F and H is more complex. The decay exponent first increases as α decrease, up to 4 for $\alpha = 0.4$. But, at the same time, both lobes decrease in size, so that one can not measure any reliable exponent for lower α values. For example, for $\alpha = 0.1$, one clearly sees on Figure 1 that both lobes (initially negative) have almost disappeared, and are replaced by slow varying positive values that are indeed located on the edges of lobes A and D or B and C .

We also studied the azimuthal variation of γ within each lobe and for different values of α . We observed that γ was independent of azimuth and lobe for $\alpha = 1$, which is in agreement with the standard prediction of linear elasticity. For $\alpha = 0.5$, the γ exponent is stable with azimuth in lobe E, F, G, H . In lobes A, B, C and D , a strong variation is observed, as γ varies between 2 and 1.5. For $\alpha = 0.1$, γ can't be determined in lobes F and H . In lobes E and G , the exponent varies from 1 on the edges to about 1.5 on its central, symmetry axis. In lobes A, B, C , and D , γ varies between 0 to about 1.8 (in lobe A , γ continuously decreases clockwise, which can be anticipated when looking at Figure 1).

These results highlight the long-range static mechanical transfer function induced by the simple asymmetric nonlinear elasticity, which may be important for long-range triggering effects between earthquakes. A full analysis of such long range triggering effect requires to take into account the other stress components, the relevant friction laws and the lithostatic and pore pressure. This will be shown in another report.

Our results open many interesting questions on the phenomenology of earthquakes that should be re-analyzed with this new non-linear perspective. In future research, an important consequence of our hypothesis of nonlinear elasticity is that stress field perturbations due to successive earthquakes can not be simply added. Stress field evolutions with time may have much sharper transitions in space and time than predicted by models involving linear elasticity, a behaviour reminiscent of the mechanics of granular media. These effects could be even stronger in mining-induced events interactions, in laboratory damage mechanics experiments as well as in volcanoes containing many cracks pressurized by cracks.

Acknowledgments: We are grateful to L. Knopoff and S. Roux for valuable information and to P. Davis, A. Helmstetter, H. Houston, J.-R. Grasso and J. Vidale for useful discussions. This work is partially supported by NSF-EAR02-30429, by the Southern California Earthquake Center (SCEC) and by the James S. McDonnell Foundation 21st century scientist award/studying complex system.

References

[1] R.S. Stein, Nature 402, 605 (1999).

- [2] A. Cochard and Madariaga R., Dynamic faulting Pure and Appl. Geophys 142, 419 (1994).
- [3] N. Lapusta, Rice, J.R., Ben-Zion, Y. and Zheng, G.T., J. Geophys. Res. 105, 23765 (2000).
- [4] D. Sornette D., P. Miltenberger and C. Vanneste, Pure and Appl. Geophys., 142, 491 (1994).
- [5] Y. Ben-Zion,Dahmen, K., Lyakhovsky, V., Ertas, D. and D. Fisher, Earth and Planet. Sci. Lett. 172, 11 (1999).
- [6] A. Gabrielov, Keilis-Borok,V. and Jackson, D.D., Proc. Natl. Acad. Sci. USA 93, 3838 (1996).
- [7] R.A. Harris, Current Science 79, 1215 (2000).
- [8] Harris, R.A., Dolan, J.F., Hartleb, R. and Day, S.M., Bull. Seism. Soc. Am. 92, 245 (2002).
- [9] R.A. Harris and Simpson, R.W., J. Geophys. Res. 103, 24439 (1998).
- [10] R.A. Harris, Simpson, R.W. and Reasenberg, P.A., Nature 375, 221 (1995).
- [11] Notwithstanding their extended use, the calculations of stress transfer have large uncertainties stemming from the usually poorly known geometry of the rupture surfaces, the unconstrained homogeneity and amplitude of the stress drop, the use of simplified models of the crust (3D semi-infinite, or thin elastic plate, or plate coupled to a semi-infinite visco-elastic asthenosphere, etc.), and the unknown direction and amplitude of the absolute stress field that pre-existed before the event.
- [12] V.I. Keilis-Borok and L. N. Malinovskaya, J. Geophys. Res., 69, 3019 (1964).
- [13] L.M. Jones and P. Molnar, J. Geophys. Res., 84, 3596 (1979).
- [14] L. Knopoff, T. Levshina, V.I. Keilis-Borok and C. Mattoni, J. Geophys. Res., 101, 5779 (1996).
- [15] S.C. Jaumé and Sykes, L.R., Pure Appl. Geophys., 155, 279 (1999).
- [16] Within the critical earthquake concept, the anomalous long-range interactions between earthquakes reflect the increasing stress-stress correlation length upon the approach of the critical earthquake [17]
- [17] S.G. Sammis and D. Sornette, Proc. Nat. Acad. Sci. USA, 99, 2501 (2002).
- [18] D. Kilb, J. Gomberg, P. Bodin, J. Geophys. Research 107, doi10.1029/2001JB000202 (2002).
- [19] J. Gomberg, J. Geophys. Res. 106, 16253 (2001)
- [20] E. Roeloffs and E. Quilty, Pure Appl. Geophys. 149, 21 (1997).
- [21] It has been argued that rock permeability and thus microcracking adjusts itself, so that fluid pressure is always close to rock pressure irrespective of the extend of hydration/dehydration [22, 23]. One possible mechanism for this involves a time-dependent process that relates fluid pressure, flow pathways and fluid volumes [24].
- [22] National Research Council, The role of fluids in crustal processes, Studies in geophysics, Geophysics study committed, Commission on Geosciences, Environment and Ressources, National Academic Press, Washington D.C. (1990).
- [23] Walther, J.V., in [22], 64.
- [24] Nur, A., and J. Walder, in [22], 113.
- [25] Much attention has been devoted to the role of overpressurized fluid [26, 27, 28, 29, 30, 31]. It is more and more recognized that fluids play an essential role in virtually all crustal processes. Ref.[32] reviews the historical development of the consciousness among researchers of the ubiquitous presence and importance of fluids within the crust. Numerous examples exist that demonstrate water as an active agent of the mechanical, chemical [33] and thermal processes that control many geologic processes that operate within the crust [22]. The bulk of available information on the behavior of fluids comes from observations of exposed rocks that once resided at deeper crustal levels. In any case, present

day surface exposed metamorphic rocks indicate that, at all crustal levels, fluids have been present in significant volume. Because the porosity of metamorphic rock is probably less than 1%, the high volume of calculated fluid necessary to produce observed chemical changes suggests that fluid must have been replenished thousands of times. It has also been proposed that gold-quartz vein fields in metamorphic terranes provide evidence for the involvement of large volumes of fluids during faulting and may be the product of seismic processes [34]. Water is also released from transformed minerals. For instance, Montmorillonite changes to illite with a release of free water from the clay structure at approximately the same depth as the first occurrence of the anomalous pore pressure [35]. This is the most commonly discussed example of hydration and dehydration of minerals changing the fluid mass and the pore pressure. Fluids have been directly sampled at about 11 km by the Soviets at the Kola Peninsula drillhole.

- [26] Lachenbruch, A.H., *J. Geophys. Res.*, 85, 6097 (1980).
- [27] Byerlee, J., *Geophys. Res. Lett.*, 17, 2109 (1990).
- [28] Rice, J.R., in *Fault mechanics and transport properties in rocks* (the Brace volume), ed. Evans, B., and T.-F. Wong, Academic, London, 475 (1992).
- [29] M.L. Blanpied, D.A. Lockner and J.D. Byerlee, *J. Geophys. Res.*, 100, 13045 (1995).
- [30] Sleep, N.H., and M.L. Blanpied, *Nature*, 359, 687 (1992).
- [31] Moore, D.E., et al., *Geology*, 24, 1041 (1996).
- [32] Hickman, S., R. Sibson and R. Bruhn, *J. Geophys. Res.*, 100, 1283 (1995).
- [33] Wintsch, R.P., R. Christoffersen and A.K. Kronenberg, *J. Geophys. Res.*, 100, 13021 (1995).
- [34] Robert, F., A.-M. Boullier and K. Firdaous, *J. Geophys. Res.*, 100, 12861 (1995).
- [35] Burst, J.P., *American Association of Petroleum Geologists Bulletin*, 53, 73 (1969).
- [36] Many observations suggest that there are massive crustal fluid displacements correlated with seismic events. Among them, one can cite the fault-valve mechanism [37] or the migration and diffusion of aftershocks [38]. Several mechanisms have been proposed for the mechanical effect of fluids to decrease compressive lithostatic stresses: mantle-derived source of fluids can maintain overpressure within a leaky fault (Rice, J.R., in [22]); laboratory sliding experiments on granite show that the sliding resistance of shear planes can be significantly decreased by pore sealing and compaction which prevent the communication of fluids between the porous deforming shear zone and the surrounding material [29]. Physico-chemical processes such as mineral dehydration during metamorphism may provide large fluid abundance over large areas [39, 40]. Such fluid presence or migration implies that cracks may open and close even at seismogenic depth, justifying the relevance of asymmetric nonlinear elasticity for such depths.
- [37] R.H. Sibson, in *Earthquake prediction, an international review*, Amer. Geophys. Union, D.W. Simpson and P.G. Richards, eds., *Maurice Ewing Ser.*, 4, 593 (1982).
- [38] A. Nur and J.R. Booker, *Science*, 175, 885 (1972).
- [39] C.H. Scholz, *The mechanics of earthquakes and faulting* (Cambridge [England]; New York: Cambridge University Press, 1990).
- [40] D. Sornette, *Phys. Rep.* 313, 238 (1999).
- [41] Many crustal rocks have a Young's modulus depending on confining pressure, in particular with a Young's modulus in tension smaller than the Young's modulus in compression in a ratio from 1/2 to 1/10 [43]. Nonlinear elasticity of rocks is also well-documented from its nonlinear wave signatures [44].

[42] In the presence of asymmetric nonlinearity, an earthquake may not be anymore a pure double-couple but may also present a dipole component corresponding to two opposite colinear forces of the same amplitude (so that the total torque is zero). The double-couple and the colinear force dipole obey the condition of mechanical equilibrium before and after the event as the total force and total torque fields exerted by the earthquake vanish.

[43] J.C. Jaeger and N.G. Cook, Fundamentals of rocks Mechanics (Chapman & Hall, London, ed. 3, 1979).

[44] R.A. Guyer and P.A. Johnson, Phys. Today, 52, 30 (1999) and other results at <http://www.ees4.lanl.gov/nonlinear/>

[45] A. Attila, Lattice dynamical foundations of continuum theories: elasticity, piezoelectricity, viscoelasticity, plasticity (Singapore: World Scientific and Taylor & Francis, 1986).

[46] This amounts to assuming a uniform and isotropic distribution of cracks with sizes smaller than the representative mesh size. Real damage in the crust is of course much more complex, with anisotropic, space and scale dependence. These complications are neglected in our first exploration. We can obtain an order of magnitude estimate of the density of fluid-filled faults associated with a given asymmetric coefficient $\alpha = K_t/K_c$, using the effective medium calculations in [47]. To simplify, let us assume $\lambda = \mu$, we have $\alpha = \lambda_1/\lambda_d = 1/(1 + 5D/2)$, where λ_1 is the Lamé coefficient of the damage material and $D = N(\ell/L)^3$ is the density of faults (assumed identical) of radius ℓ in a cube of volume L^3 . N is the number of faults in that volume. For instance, we need about 11 faults of size $L/3$ to get $\alpha = 0.5$. Such estimate must however be taken with caution since the effective medium calculation $\alpha = 1/(1 + 5D/2)$ is valid only for small crack densities, while any piece of rock and the real crust are crisscrossed by many faults at many length scales, most of them being healed at varying degrees. We think that values of α significantly smaller than 1 should thus not be excluded.

[47] H.D. Garbin and L. Knopoff, Q. appl. Math. 33, 301 (1975).

[48] L. Monette and M. P. Anderson, Modelling Simul. Mater. Sci. Eng. 2, 53 (1994).

[49] We solve for the node displacements by an iterative relaxation method. During each iteration, all nodes are sequentially considered. For each node, the total force exerted on it by all connected springs (plus the possible external force) is computed, and the node is moved in the direction of the net force so as to decrease its amplitude. We sweep the network alternatively from right to left and from left to right, from top to bottom and from bottom to top. Upon iterating, the net force acting on any node decreases until a threshold is reached and we stop the computation and consider the resulting displacement field as the correct equilibrium one. The threshold is chosen so that the displacement necessary to lower the net force on a node becomes comparable to the numerical accuracy. We have verified that our results in the scaling region of distances r larger than the mesh size a but no larger than $L/5$ are independent of the boundary conditions and of the plate size L and are robust with respect to the choice of the arrest criterion. Most of our calculations have been performed with $L = 50a$ to $200a$ and we report our results for $L = 200a$.

[50] G. Peltzer, F. Crampé and G. King, Science 286, 272 (1999).

[51] The Manyi fault surface rupture has an average orientation $N76 - E$. From Figure 1, for a left-lateral strike-slip fault, we see that the closest dynamic nodal plane should be obtained from the geometrical rupture plane by an anti-clockwise rotation. Three inversions of the focal mechanism of the Manyi earthquake have been performed, which provide three dynamic planes close to the geometrical rupture plane: Harvard CMT (with a plane oriented $N79 - E$), Moscow ($N84 - E$), and NEIC ($N70 - E$). If these rotations are genuine, the first two planes correspond to clockwise rotations of the observed static plane, which contradict our theory. In contrast, the NEIC solution finds a 6° clockwise rotation from the rupture plane. Assuming this solution as the genuine one, this rotation corresponds to an asymmetric ratio $\alpha = 0.5$ as seen in Figure 2. This value is close to the rough estimate of Peltzer et al. [50] obtained from independent data. While this is encouraging, this does not explain why the two other

solutions of Harvard CMT and Moscow disagree. Other problems may be due to the fact that the dynamical rupture mechanism is more complex and has occurred on a more complex geometry. Coupled with possible nonlinear elasticity, this would considerably entangle the relationship between static and dynamic planes. Additional effects include the free surface and the coupling with the lower crust.

- [52] Lobes A, B, C and D exhibit a slight rotation as α is decreased. Lobes A and C rotate clockwise, while lobes B and D rotate counter-clockwise as α decreases. The initial square geometry is thus broken by the nonlinear elasticity but the shear stresses within these lobes remain approximately of the same amplitudes. Lobes E, F, G and H exhibit a spatial structure which is not the symmetric of the lobes A, B, C and D . Thus, not also is the square symmetry broken within the class of lobes of the same sign, but it is also broken between the two families. As α decreases, lobes E and G widen while lobes F and H become narrower. Moreover, the two couples of lobes remain orthogonal to each other for all values of α . They still wear the fingerprint of the tensile and compressive quadrants of the double-couple.
- [53] M.E. Cates, Wittmer J.P., Bouchaud J.-P., Claudin P., *Phys. Rev. Lett.* 81, 1841 (1998).
- [54] Ref. [55] gives the analytical solution for the stress field and for the dependence $\gamma(\alpha)$ in a nonlinear asymmetric elastic medium in the case of antiplane mode III loading, which is thus the scalar equivalent to the problem studied here. In the antiplane case, there is only one stress component and a single exponent $\gamma(\alpha)$.
- [55] S. Roux and F. Hild, *Int. J. Fract.* 116, 219 (2002).

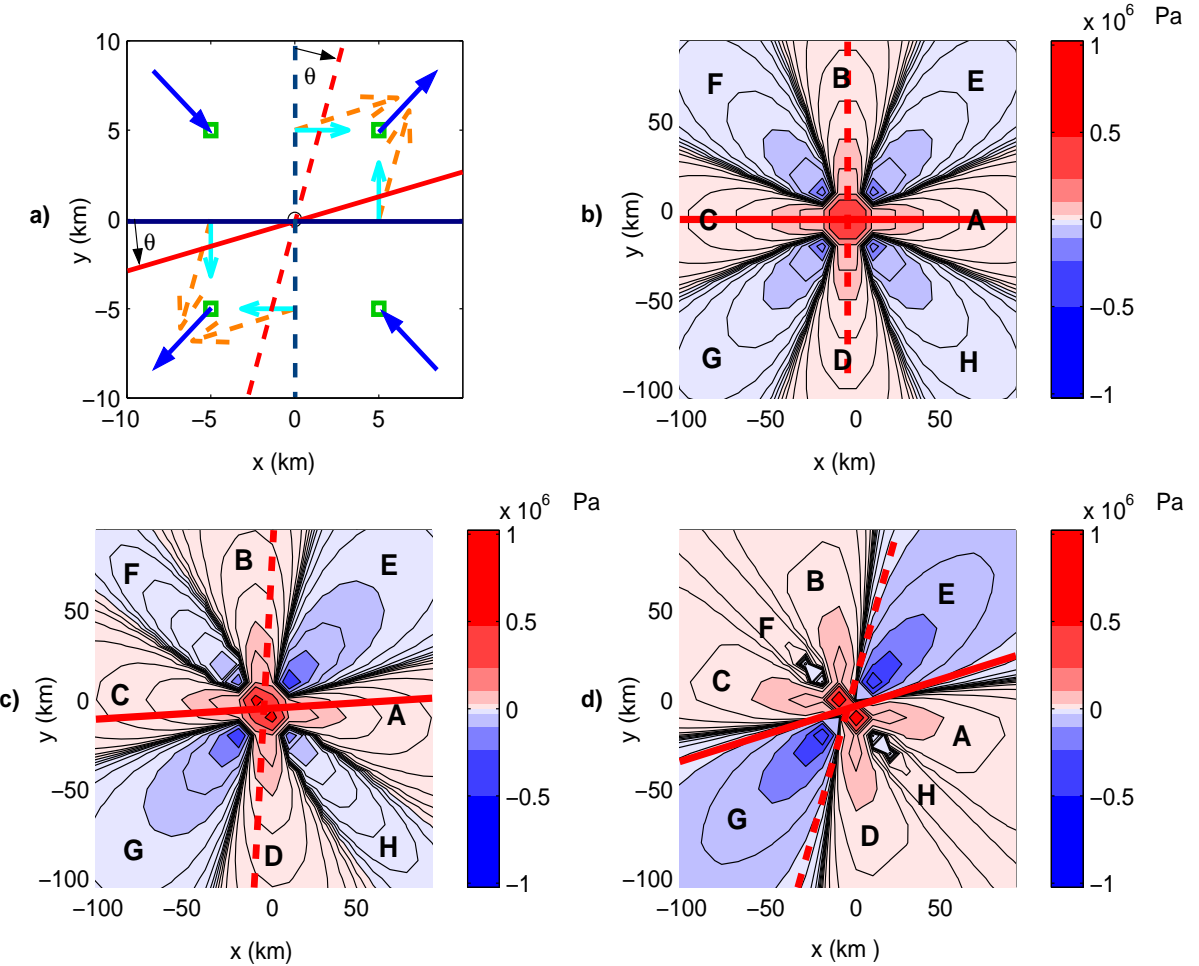


Figure 1: Distances are given in hundreds of kilometers. a) The continuous blue arrows show the four forces (each of modulus F) defining the double-couple earthquake applied to the nodes (green squares) of a single cell. This defines a positive shear stress σ_{xy} at the source. The orange dashed-line arrows give the corresponding orientation of the displacement field interpolated on the vertical and the horizontal axes of the point-wise source (shown as a black circle), which define two conjugate fault discontinuities shown as the two red thick solid and dashed lines, for an asymmetric ratio $\alpha \equiv K_t/K_c = 0.1$. K_t (respectively K_c) is the elastic modulus in tension (respectively compression). The right-lateral discontinuity is shown as the red continuous line, while the left-lateral discontinuity is shown as the red dashed line. The real fault plane should thus be along one of those two lines. The cyan continuous arrows show the displacement directions interpolated at the same locations as above, but in the linear case. The right-lateral and left-lateral nodal planes are shown respectively as continuous and dashed thick blue lines. For $\alpha < 1$, due to the asymmetric nonlinear elasticity, the pair of fault discontinuities doesn't match, as they are rotated by an angle θ (clockwise for the left-lateral plane, anticlockwise for the right-lateral plane). b) σ_{xy} increment due to the double-couple for $\alpha = 1$. See a) for definition of red lines. Contour lines are spaced by a factor 2. Red lobes are subjected to stress increase, blue lobes to stress drop. c) Same as b) for $\alpha = 0.5$. d) Same as b) for $\alpha = 0.1$.

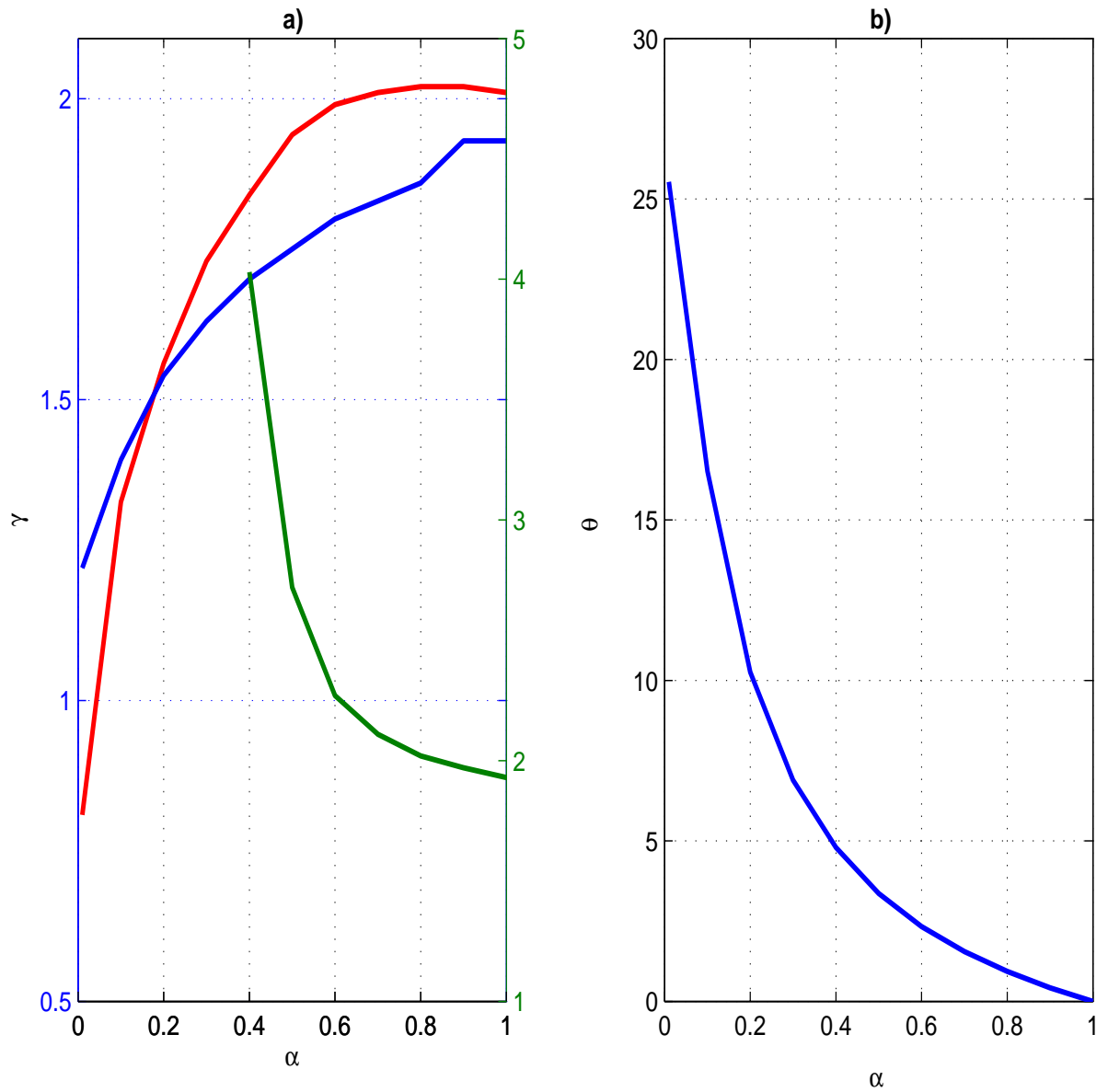


Figure 2: a) Dependence of the exponent γ with α . γ is the exponent of the power law describing stress decrease as a function of distance. The red (respectively blue) curve is for lobes A, B, C, D (respectively E, G); their scale is shown on the left vertical axis. The green curve is constructed for lobes F, H, with scale on the right vertical axis. b) Dependence of the angle θ between the geometrical displacement discontinuity and the nodal planes of the double-couple as a function of the asymmetric ratio α .

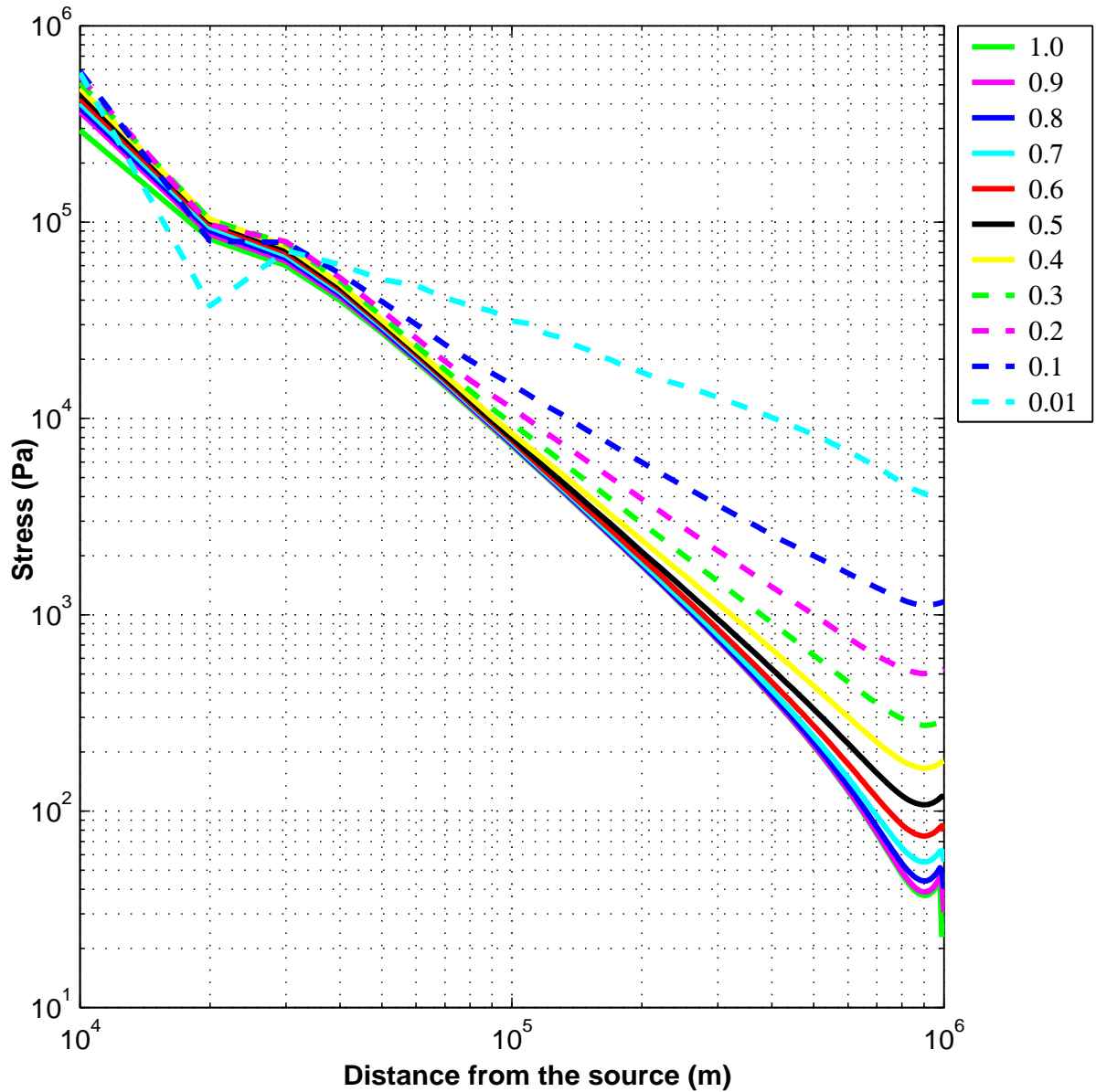


Figure 3: Power law decrease in $\log - \log$ scale of the shear stress σ_{xy} as a function of distance from the earthquake source for different values of α (from 0.01 to 1 - see insert on top right for the color code), measured on the crest of lobes A, B, C, D . Clear power law regimes can be observed for distances between 40 km and 300 – 400 km. Deviations from a pure power law occur far from the source (due to boundary effects) and close to the source (because of its finite size and of lattice effects).